International Research Journal of Engineering and Technology (IRJET) e-ISSN: 2395-0056
Volume: 09 Issue: 07 | July 2022 www.irjet.net p-ISSN: 2395-0072

PERFORMANCES OF DİFFERENT OPTİMİZATİON METHODS FOR CALİBRATİNG OF THE COMBİNED HARDENİNG RULE'S PARAMETERS FOR WİRE DRAWİNG SİMULATİON

Burak DEVECIOGLU[1], Erhan CELIK[2], Merve ERTUGRUL[3]

[1]*Master Student, Nigde Omer Halisdemir University, Department of Mechanical Engineering, 51245 Niğde, Turkey*
[2]*Graduate Student, Nigde Omer Halisdemir University, Department of Mechanical Engineering, 51245 Niğde, Turkey*
[2]*Student, Nigde Omer Halisdemir University, Department of Mechanical Engineering, 51245 Niğde, Turkey*

Abstract – *Plasticity models were developed in this study to be used in simulations of the wire drawing process of the AA7075-T6 alloy, which has many applications. Furthermore, the obtained model's coefficients were calibrated using the genetic algorithm optimization method. The hardening rule in the models combines Chaboche nonlinear kinematic and bilinear isotropic hardening rules. The associated flow rule, the Hill48 yield criterion, and the hardening rules were used to obtain plasticity models. As a result, the most suitable strain hardening model for monotonic loading deformation cases is presented and the effects of parameters on simulation results are shown.*

Key Words: Wire Drawing, The Chaboche Kinematic Hardening Model, AA7075-T6, Bilinear Isotropic Hardening Model, Finite Element Analysis, ANSYS

1.INTRODUCTION

Today, wire is primarily utilized for circular items and is used practically everywhere. The major applications for wire are conductor and resistance wires, as well as the packaging sector, springs, nails, rivets, chains, and ropes. It is depicted in the play as well. It is also seen in the production. Reducing the cross section of the wire through a die is the process of wire drawing. Wire sections are generally produced in circular form. However, square, hexagonal, and different geometries can be drawn according to the area and requirements to be used. In terms of lubrication, the drawing process is divided into dry and wet. Grease or soap powder is used for dry shrinkage, and liquid oil is used for wet shrinkage.

The purpose of the extrusion process is to obtain improved durability, strength, flexibility, and a smooth outer surface. Therefore, the behavior of the material during manufacturing, mold geometry, lubricant, shrinkage rate, and the parameters that develop depending on these factors are of great importance to us. Figure 1 shows the basic process variables of the wire drawing process. The main advantage of the finite element method is its ability to provide detailed information such as stress values, temperatures, contact pressure distribution, and strain.

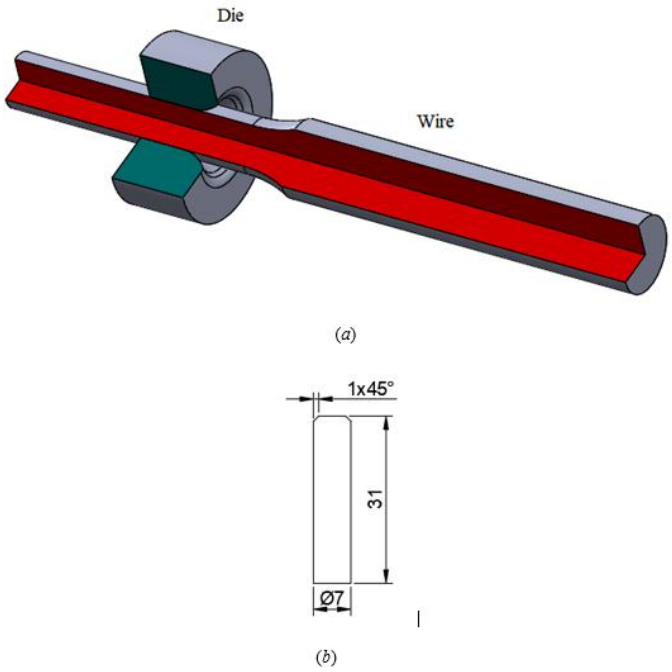

Figure 1. (a) Schematic illustration of wire drawing (b) Wire dimensions (units in mm)

In this study, finite element analysis of the tensile process of wires made of AA7075 T6 alloy, which is widely used in the manufacturing industry, has been carried out. Bilinear and Chaboche models were used to model the plastic behavior of the wire. The coefficients of the models were calibrated using the genetic algorithm optimization method. Plasticity models were obtained by using the associated flow rule and Hill48 yield criterion besides the consolidation rules.

In the current studies in the literature, the finite element method was used to simulate the wire drawing process, and the effects of tensile force and die geometry on the drawn wire were determined [1]. Simulations of the wire drawing process and optimization of geometric formwork are commonly performed. The effects of the tensile force on the process parameters such as die wear, lubrication [2], friction coefficients [3] and material thinning were determined [4-6]. As a material model, the effects of hardening and non-

hardening material models on the wire drawing process are examined and a comparison is made between analytical methods and the finite element method. [7]. The relationship between friction coefficient, die angle, and rod diameter was determined by examining the radial stresses on the drawn wire surface. By classifying in detail the types of inclusions that cause damage in wire drawing operations, it has been demonstrated that chemical alopecia containing alumina and silicate are the main causes of damage [8]. The ability to perform the simulations in a realistic way affects the usability of the found values in the first degree. Unfortunately, there is not yet a single model that can be used for all plastic deformation processes and is suitable for all types of materials. In this case, it has been found that isotropic and/ or kinematic models [9-11] are often used in combination for simulations of tensile processing. It will not be sufficient alone for repeated load cases of the loading type.

Experimental stress values were compared with those obtained from the models. As a result, the most suitable hardening model for monotonic and cyclic loading deformation cases is presented, and the effects of model parameters on deformation estimation are shown.

3. EXPERIMENTAL TENSILE TESTS AND CHARACTERIZATION OF AA7075-T6

3.1. Chemical Composition

The material of the wire is AA7075-T6. Its elemental composition is given in Table 1[12].

Alloy	Zn	Mg	Cu	Cr	Fe	Ti
7075	5.209	2.174	1.876	0.257	0.263	0.044

Mn	Al
0.086	Bal.

3.2. Monotonic Tensile Test and Bilinear Isotropic Hardening Rule

As shown in Figure 2*a*, monotonic stress and strain curve were obtained in the coordinate system using plate samples prepared according to the ASTM E8 standard.

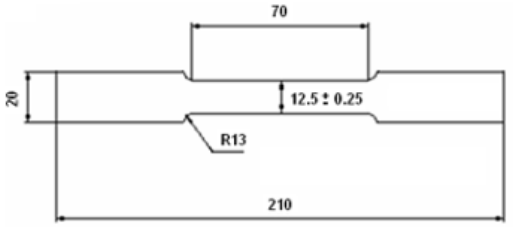

a) Geometry of the sample for monotonic tensile testing (units in mm)

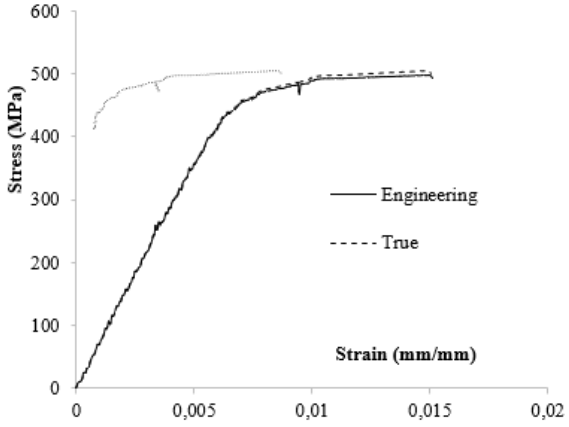

b) Stress-strain relationship of sample for monotonic tensile test

Figure 2. Monotonic tensile test and results

The tests were performed on a Shimadzu Autograph 100 kN test machine with a data acquisition system held by a digital interface card using a special computer program. Sample elongation was measured by a video-type extensometer measuring system. The result of the monotonic tensile test is shown in Figure 2. The mechanical properties of AA7075-T6 are shown in Table 2.

Table 2. Mechanical properties of AA7075-T6

Density	2.81 g/cm^3
Elasticity Module	71.7 GPa
Poisson Ratio	0.33
Yield Strength	372 MPa
Maximum Strength	572 MPa
r_0	0.383
r_{45}	0.692
r_{90}	0.474

Parameters of bilinear isotropic hardening model; yield strength (YS) and tangent modulus Et; on the data obtained from the monotonic tensile test; elastic deformation is removed and determined using true stress-true plastic deformation values [13]. Elastic deformation from these values is explained in detail by Kacar and Kılıç (2018) [14]. In this study, the bilinear isotropic consolidation rule is combined with Chaboche's nonlinear kinematic hardening rule.

3.1. Low Cycle Hysteresis Loop

The parameters of the Chaboche hardening rule are yield strength (YS) and material constants C_m, γ_m;on data obtained from one stable cyclic loading cycle (strain controlled and symmetrical) in the form of loading-unloading-reverse-loading; Elastic deformation is eliminated and the actual stress-true plastic deformation values are determined by applying curve fitting algorithms based on nonlinear regression. Sprains should be delayed [15]. Kacar and Toros (2016) revised the retaining system of the test setup and developed a new retainer to modify the ASTM E8 type of specimens to fit this new setup and thus ensure that the buckling modes are adequately delayed [16]. In this study, this mechanism and sample type were used. The dimensions of the samples are given in Figure 3.

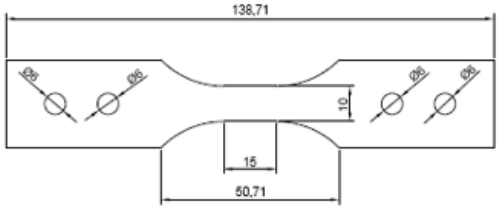

Figure 3. Sample geometry for low cycle hysteresis loop test (units in mm)

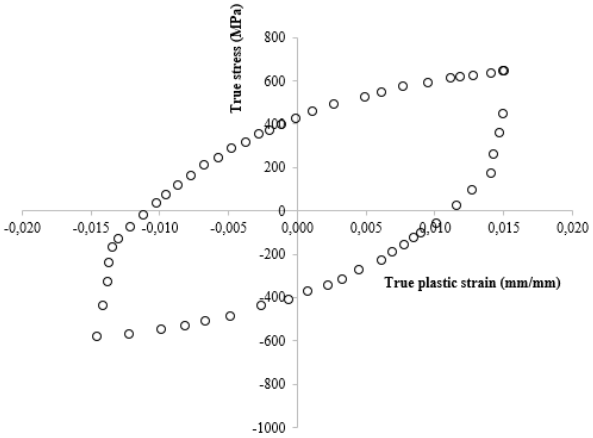

Figure 4. True stress true plastic deformation diagram obtained from cyclic uniaxial tensile testing for AA7075-T6 at room temperature

Figure 4 shows a stable cycle obtained at room temperature using a symmetrical strain controlled loading method. The deformation range is ± 0.015 and the deformation ratio is R = −1.

4. CONSTITUTIVE EQUATIONS

The deformation of the wire drawing process was simulated. Stress and deformation amounts were determined. In the finite element method, structural equations are needed to simulate the trans-elastic behavior of the material. In this study, the related flow rule [17], Hill48 yield criterion [18], and hardening models were used to form the constitutive equation. As reinforcement models; bilinear isotropic, Chaboche kinematics, and combination models were used.

4.1. Yield Critertion

The yield criterion specifies a boundary surface in the principal stress space. This limit defines whether the material shows flow. A general formula for the yield criterion is given in Equation (1).

$$\bar{\sigma}(\sigma_{ij}) - \sigma_0 = 0 \qquad (1)$$

σ_0 is the yield strength of the material. It is the simplest form and does not have curing effects. The Hill48 yield criterion is used in this study. The equivalent stress expression of the Hill48 yield criterion for a general stress state is given in Equation (2).

$$\emptyset(\sigma_{ij}) = F(\sigma_{yy} - \sigma_{zz})^2 + G(\sigma_{zz} - \sigma_{xx})^2 + H(\sigma_{xx} - \sigma_{yy})^2 + 2L\sigma_{yz}^2 + 2M\sigma_{zx}^2 + 2N\sigma_{xy}^2 \quad (2)$$

Here, σ_{ij}, i , j=x, y, z represent the generalized stress state at a point on the structure. $\bar{\sigma}$ is the coefficients related to anisotropy values of the yield criterion G, H, F, L, M, and N as in the equation of equivalent stress expression and r_0, r_{45}, r_{90} is given in Equation (3).

$$F = \frac{r_0}{r_{90}(r_0+1)}, \quad G = \frac{1}{r_0+1},$$
$$H = \frac{r_0}{r_0+1}, \quad N = \frac{(r_0+r_{90})(1+2r_{45})}{2r_{90}(1+r_0)} \qquad (3)$$

If the equation is rewritten using the stress values $\sigma_1, \sigma_2, \sigma_3$, Equation (4) is obtained.

$$\emptyset(\sigma_{1,2,3}) = F(\sigma_2 - \sigma_3)^2 + G(\sigma_3 - \sigma_1)^2 + H(\sigma_1 - \sigma_2)^2 = \bar{\sigma}^2 \qquad (4)$$

If these coefficients are calculated, F = 0.584249369, G = 0.723065799, H = 0.276934201, and N = 0.330105567. In our study, we used only the F, G, *and* H coefficients because we are dealing with prime stresses. Calculated in line with r_0= 0.383, r_{45}= 0.692, r_{90}= 0.474.

4.2. Hardening Rule

When the flow begins during the plastic deformation process, hardening or softening occurs due to the

displacement, that is, the dislocation of the movements. Isotropic hardening rule in determining the expansion or contraction of yield surfaces, the kinematic hardening rule provides that the yield surface α_{ij} be postponed until the center point. A yield surface general formula containing the terms of hardening is given in Equation (5).

$$\bar{\sigma}(\sigma_{ij} - \alpha_{ij}) - \sigma(h) = 0 \qquad (5)$$

The term *σ(h)* isotropic hardening, and the term α_{ij} is called back stress. Prager, Ziegler, Armstrong Frederic, Chaboche, Yoshida Uemori have several σ_{ij} functions. In this study, Equation (6), given the bilinear isotropic hardening rule [19], and Equation (7), given Chaboche's nonlinear kinematic hardening rule [20], were used separately and combined.

$$\sigma(h) = YS + TM(\varepsilon^p) \qquad (6)$$

YS is yield strength, and *TM* is the tangent modulus, and ε^p is the actual amount of plastic deformation.

$$(\dot{\alpha}_{ij})_m = \underbrace{\frac{2}{3}C_m\dot{\varepsilon}^p_{ij}}_{linear\ term} - \underbrace{\gamma_m(\alpha_{ij})_m\sqrt{\frac{2}{3}\dot{\varepsilon}^p_{ij} : \dot{\varepsilon}^p_{ij}}}_{the\ plastic\ strain\ range\ memorization\ term} +$$

$$\underbrace{\frac{1}{C_m}\frac{\partial C_m}{\partial T}(\alpha_{ij})_m\dot{T}}_{heat\ rate\ term} \quad where\ m = 1,2,\dots n \qquad (7)$$

Where *m* = 1,2, …, *n* where *n* is the total number of terms, *T* is the temperature, and C_m is the consolidation modulus for the *m*'th term. In addition, γ_m is a unitless value calculated by the slope of the curve, which indicates the rate of reaching the threshold value and means a reduction rate of consolidation. These parameters may be different for each term. $\dot{\varepsilon}^p_{ij}$ is the cumulative plastic deformation ratio and will be obtained by a flow rule. All of these parameters are determined by a nonlinear regression process applied to a regular hysteresis cycle. The regression is applied to the true stress-true plastic deformation cycle obtained from the low cycle stress compression type fatigue test.

Equation (7) is the first-order ordinary differential equation and must be solved. The scope of this study will be obtained as in Equation (8) when Chaboche's first-order inverse stress equation is solved by integrating $\dot{\varepsilon}^p_{ij}$ with the assumption that there is no temperature change ($\dot{T} = 0$).

$$\alpha = \varphi\frac{C}{\gamma} + \left(\alpha_0 - \varphi\frac{C}{\gamma}\right)e^{-\varphi\gamma\left(\varepsilon^p - \varepsilon^p_0\right)} \qquad (8)$$

Where α_0 is the inverse stress value at the beginning of flow, ε^p_0 is the initial plastic deformation value, and φ is a sign indicating the direction of loading, calculated by φ = sgn (σ-α) = ± 1. There will be φ = 1 for uniaxial drawing and φ = -1 for pressing. If a sample does not have any pre-deformation at the beginning of the tests, the initial inverse stress will be α_0 = 0and the initial plastic deformation value ε^p = 0. Thus, inverse stress equations, Eq (9).

$$\alpha = \frac{C}{\gamma}\left(1 - e^{-\gamma(\varepsilon^p)}\right) \quad \text{for tension case} \quad (9a)$$

$$\alpha = \frac{C}{\gamma}\left(-1 - e^{-\gamma(\varepsilon^p)}\right) \quad \text{for compression case} \quad (9b)$$

When we replace the inverse stress equation of Chaboche in the equivalent stress expression in the yield criterion, $\bar{\sigma}(\sigma_{ij} - \alpha_{ij}) - \sigma(h) = 0$ will generally be included in the yield criterion. In the case of a uniaxial tensile test, the equivalent stress will only be equal to the normal stress in the x tensile axis, ie $\bar{\sigma}(\sigma_{ij}) = \sigma_x$. Thus, the equivalent stress formula in the yield criterion will become $\bar{\sigma}(\sigma_x - \alpha_x) - \sigma(h) = 0$ The yield criterion can be rewritten as in Equation (10) for uniaxial loading in the x direction.

$$\sigma_x - \alpha_x - \sigma(h) = 0 \qquad (10)$$

Equations (9) and (10) flow by using uniaxial loading status, which will have comprised the combined hardening rule.

$$(\sigma_x)_{tension} = \sigma(h) + \frac{C}{\gamma}\left(1 - e^{-\gamma(\varepsilon^p_x)}\right)$$

$$for\ tension\ case \quad (11a)$$

$$(\sigma_x)_{compression} = -\sigma(h) + \frac{C}{\gamma}\left(-1 + e^{\gamma(\varepsilon^p_x)}\right)$$

$$for\ compression\ case \quad (11b)$$

More than one term for more realistic simulations of the plastic deformation processes, in particular when subjected to multiple repetitions, and, if possible, the more cycles the draft object is actually exposed to. The increase in the number of terms in the Chaboche equation gives more accurate results in such successive loads. Therefore, if we write the Chaboche inverse stress equation for three terms, the following equations will be obtained.

$$\alpha = \sum_{m=1}^{3}(\alpha)_m = (\alpha)_1 + (\alpha)_2 + (\alpha)_3 \qquad (12)$$

$$\alpha_1 = \frac{C_1}{\gamma_1}\left(1 - 2e^{-\gamma_1\left(\varepsilon^p - \varepsilon^p_L\right)}\right) \qquad \text{for tension case (13}a\text{)}$$

$$\alpha_2 = \frac{C_2}{\gamma_2}\left(1 - 2e^{-\gamma_2(\varepsilon^p - \varepsilon_L^p)}\right)$$

$$\alpha_3 = C_3\varepsilon_{Lx}^p$$

$$\alpha_1 = \frac{C_1}{\gamma_1}\left(-1 + 2e^{\gamma_1(\varepsilon^p - \varepsilon_L^p)}\right)$$

$$\alpha_2 = \frac{C_2}{\gamma_2}\left(-1 + 2e^{\gamma_2(\varepsilon^p - \varepsilon_L^p)}\right) \quad \text{for compression case (13}b\text{)}$$

$$\alpha_3 = -C_3\varepsilon_{Lx}^p$$

As it can be inferred from these statements, the term $\gamma 3$ does not exist in this equation and the term $\gamma 3$ is used for racheting estimates that are outside the scope of this study. $\gamma 3$ terms alone are not sufficient to determine the hysteresis loop. Another tensile-compression test consisting of several cycles with tensile control is required, and a small positive value of $\gamma 3$ can generally be given [21].

If Equation (13) is substituted in Equation (10), the yield criterion will now contain the consolidation rules, as can be seen in Equation (14). In this case, the subscripts *t* and *c,* respectively, show the tensile and compression states.

$$(\sigma_x)_{t/c} = \pm\sigma(h) \pm \frac{C_1}{\gamma_1} \pm \frac{C_2}{\gamma_2} \pm C_3\varepsilon_{Lx}^p \qquad (14)$$

4.3. Flow Rule

The flow rule is required to calculate the direction of the plastic strain increase (ε_{ij}^p). The flow rule shows how much equivalent plastic deformation (ε_e^p) is seen during material flow. It also shows the relationship between plastic stress and stress. The general equation of a flow rule is $d\varepsilon_{ij}^p = d\lambda \frac{\partial f}{\partial \sigma_{ij}}$, where λ is the plastic multiplier. *f* is a scalar function and is also called "plastic potential". In this study, the flow criteria function is taken as the plastic potential function. This acceptance is called the associated flow rule and is a general case for metallic materials [22].

5. Finding Parameters

As a result of the nonlinear regression process, the yield strength of the bilinear isotropic hardening model was obtained by using *YS* and tangent modulus E^t and *YS*, C_m, γ_m parameters found in the Chaboche equation. Yield values (*YS*) in both models are common. In this study, a three-term Chaboche equation was used.

Table 3. Parameters of the models calculated by regression (from monotonic values)

	Bilinear isotropic hardening		Chaboche's kinematic hardening					
Model	E^t (MPa)	*YS*(MPa)	C_1(MPa)	γ_1	C_2(MPa)	γ_2	C_3(MPa)	γ_3
Bilinear	7971.37	449.57	--	--	--	--	--	--
Chaboche	--	387.93	23271.77	603.96	23267.33	579.44	23267.44	609.32
Combine	731.55	386.18	24285.37	658.92	24290.62	637.48	24290.90	637.45

Table 4. The parameters of the models calculated by regression (from cyclic values)

	Bilinear isotropic hardening		Chaboche's kinematic hardening					
Model	E^t (MPa)	*YS*(MPa)	C_1(MPa)	γ_1	C_2(MPa)	γ_2	C_3(MPa)	γ_3
Bilinear	5193.82	116.46	--	--	--	--	--	--
Chaboche	--	243.59	9217.83	-14.86	9931.12	61.37	9931.07	61.22
Combine	1718.24	243.59	19838.01	188.66	19838.35	190.70	19585.50	45.85

As can be seen from the tables, while a hardening rule for AA7075-T6 material stands alone, the calculated parameters are different from each other. In addition, different coefficients are obtained in monotonic or cyclic data cases.

5.1. Optimization For Calibration of Hardening Model Parameters

The fact that the model parameters are found by curve fitting does not mean that the parameters obtained will comply with all kinds of plastic deformation processes. Optimization processes are frequently used for this purpose. The initial material constants *YS*, E^t, *C1*, γ_1, *C2*, γ_2, *C3*, γ_3 are defined as the input values of the optimization process. As in Equation (15a), an objective function is determined. For the optimization process, first design points are determined and a solution is obtained for the design points obtained in Equation (15*b*, *c)*. In order to see the relationship between the obtained results and variables, the Kriging [23] method can be used to graph the input values and output values and follow the changes before optimization.

$$F(x) = \Phi(x)\,pred - \Phi exp \rightarrow min. \qquad (15a)$$

$$\text{Lower boundry} \leq x \leq \text{Upper boundry} \qquad (x \in R) \qquad (15b)$$

$$\text{Lower boundry} \leq x \leq \text{Upper boundry} \qquad (15c)$$

The mathematical meaning of the optimization process, numerical estimation and deformation, deformation, stress, and so on. is the minimum search for the difference between experimental measurements of variables. The best parameters that can bring the difference to zero or near zero will be a point to the optimum value. At the end of a

successfully completed optimization, the estimation of the model with optimized constants should best match the experimental measurement. FE analysis software was used for both simulation and optimization [20]. Tables 5 and 6 show the upper and lower limits of the parameters to be optimized. In Table 7, the parameters of the GA method used for optimization are given.

Table 5. Lower and upper limits of design variables for monotonic loading

	E^t (MPa)	YS(MPa)	C_1(MPa)	γ_1	C_2(MPa)	γ_2	C_3(MPa)	γ_3
Initial value	731,55	386,18	24285,37	658,92	24290,62	637,48	24290,90	637,45
Lower limit	630,00	280,00	23000,00	550,00	23000,00	530,00	23000,00	530,00
Upper limit	830,00	480,00	25000,00	750,00	25000,00	730,00	25000,00	730,00

Table 6. Lower and upper limits of design variables for cyclic loading

	E^t (MPa)	YS(MPa)	C_1(MPa)	γ_1	C_2(MPa)	γ_2	C_3(MPa)	γ_3
Initial value	1718,24	60,62	19838,01	188,66	19838,35	190,70	19585,50	45,85
Lower limit	1610,00	40,00	18000,00	88,00	18500,00	90,00	18500,00	35,00
Upper limit	1820,00	75,00	20500,00	280,00	20500,00	290,00	20500,00	55,00

Table 7. GA's parameters used in the optimization.

Parameters	Value
Estimated number of evaluation	2000
Number of initial samples	100
Number of samples per iteration	100
Maximum allowable pare to percentage	70%
Convergence stability percentage	2%
Maximum number of iterations	1000

5.2. Meshing, Boundary Conditions, And Numerical Results

5.2.1. Monotonic Drawing Process

In finite element analysis, an axial symmetric 2D model is used instead of a 3D model to avoid time-consuming calculations. The cylindrical coordinate system (x, θ, z) is located at the center of the wire. The axial symmetry axis of the finite element model is located on the y axis. The radial direction corresponds to the x direction. As shown in Figure 5, the symmetrical model is placed in the positive x direction considering the radial dimensions.

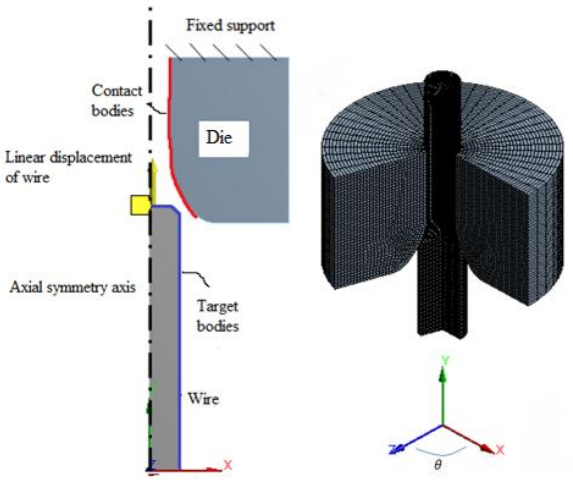

Figure 5. An axially symmetrical model of wire drawing

The mold and wire models were separated using i square-shaped elements. The friction between the die and the wire was taken as 0.125 to simulate metallic metal contact. The mold is fixed to the surface shown in the figure with a built-in bracket and is modeled as rigid. Wire material is modeled as a deformable object using AA7075-T6 material with the data in Tables 1 and 2. A displacement in the y direction is defined by restricting the movement of the wire in the x direction. As shown in Figure 6b, this linear displacement was applied in a total of 181 steps. Our aim here is to pull the 7 mm diameter wire from the 5 mm diameter mold cavity. To avoid convergence problems, the wire is placed a little behind the contact point of the mold. This behavior prevents excessive deterioration or detachment of the elements from the contact surfaces. Furthermore, when deformation was applied to the end of the wire, a bending problem occurred during the passage of the die mist. In order to overcome this, deformation steps were applied to the bevelled surface by chamfering the end portion of the wire, thus eliminating the convergence problem.

The wire moves into the mold by moving in the + y direction, as indicated in Figure 6b. A total displacement of 90.5 mm was defined. It is important to note here that the length of the wire will be shorter as the length will be shortened. The model is confirmed by comparing the experimentally measured and estimated values of the diameter of the drawn wire. It is then used as input data for the next step, the optimization process, to calibrate the material parameters to give the closest result to the experimental value.

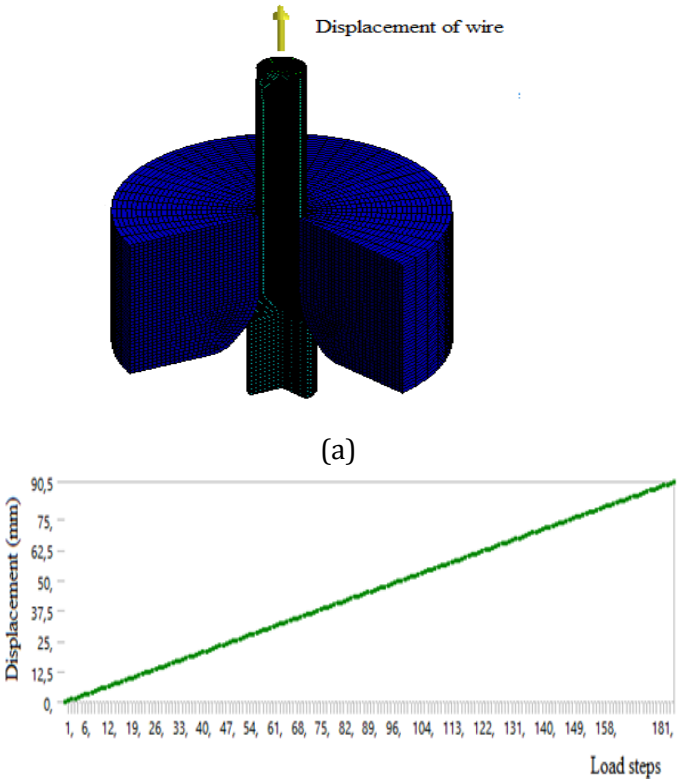

(a)

(b)

Figure 6. (*a*) Finite element model for simulation of monotonic plastic deformation, (*b*) displacement steps applied to the wire

The parameters in Tables 3 and 4 are used as initial values for the constants of the material models of AA7075-T6. Although the diameter of the mold is 5 mm, there are minor deviations in the diameter of the drawn wire exiting the die due to the spring-back. The figures show the last step solutions for all geometry.

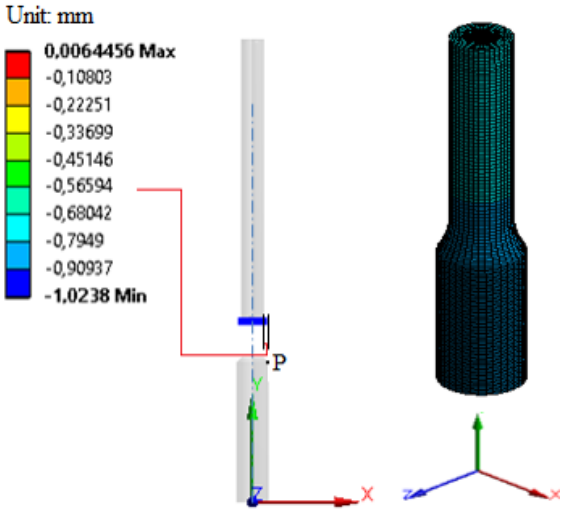

(a)

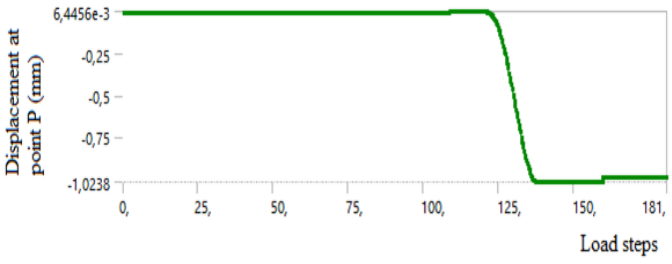

(b)

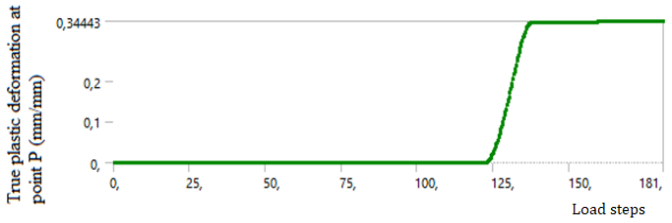

(c)

Figure 7. (a) The combination of bilinear isotropic and Chaboche kinematic model results in deformation at the last stage in the x direction (b) displacement at point P (c) actual plastic deformation of point P

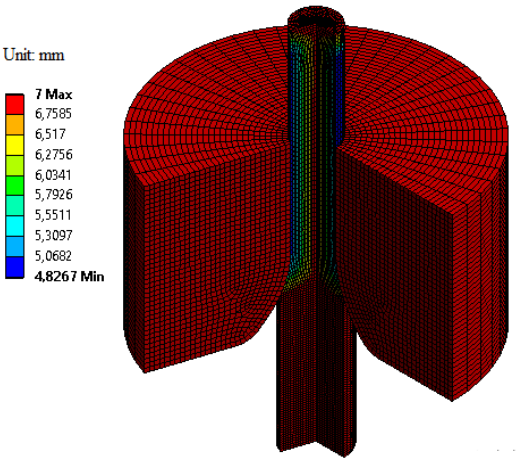

(a)

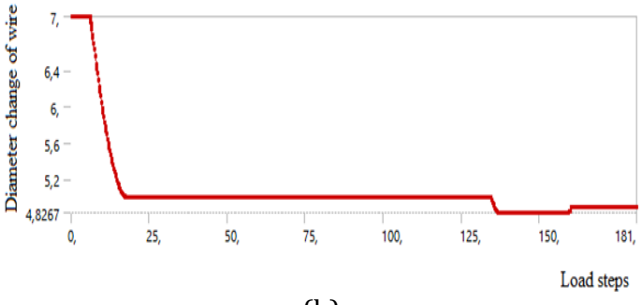

(b)

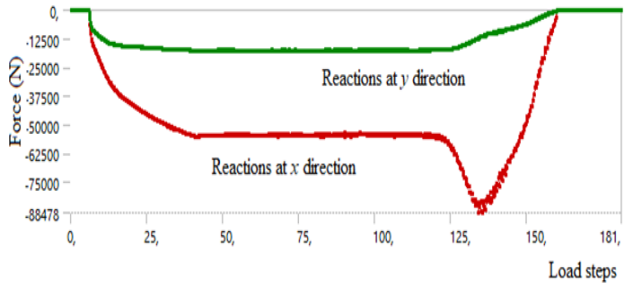

(c)

Figure 8. (a) Change in wire diameter during the process (mm) (b) Change in diameter according to load steps (c) Bearing reactions

5.2.2. Cyclic Draw/ Press Operation

Model parameters to be calculated for cyclic operating conditions must be obtained using a cyclic process. For this reason, the model shown in Figure 10 was used to perform a separate analysis for the cyclic state. The difference between the model and the model in the wire drawing process is that the displacement is not applied directly to the surface. The displacements were applied at 31 levels in total. The solution lasted 3 min 52 sec. Both positive and negative displacement were applied to the top surface of the wire. In this way, the displacements are applied without leaving the surface of the wire. The applied displacement and the obtained permanent deformation values are shown in Figure 9 b and c. As can be seen from Figure 11c, a displacement between 1.53 mm and -1.25 mm is required as in Figure 9'b in order to produce ± 0.015 deformations. The stress distribution resulting from the displacements applied is shown in Figure 10. The combined model in Table 4 was used for the analysis.

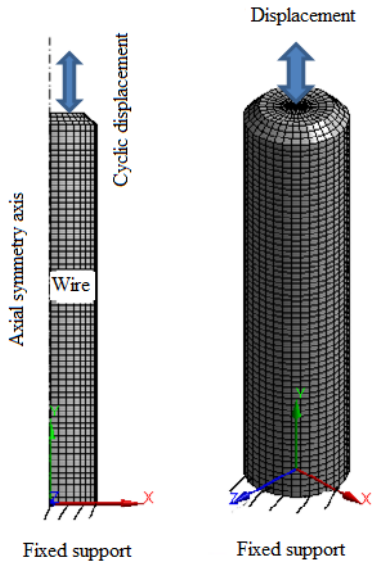

(a)

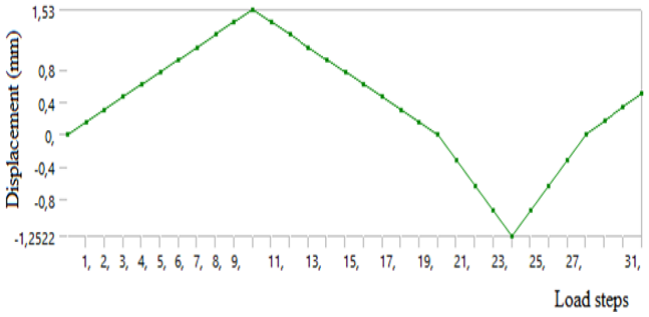

(b)

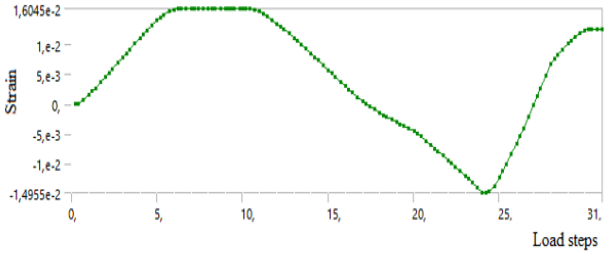

(c)

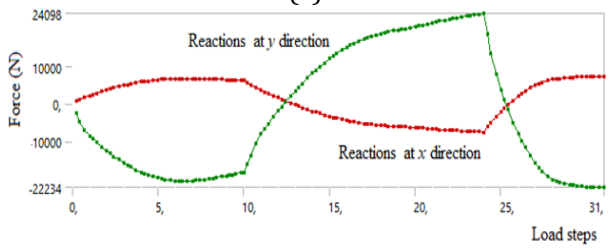

(d)

Figure 9. (a) FE model for cyclic plastic deformation simulation, (b) Wire displacement steps, (c) Permanent deformation of wire and (d) Bearing reactions

As can be seen from Figure 9*b*, a displacement between (1.53mm) - (- 1.25mm) boundaries is required as in Figure 9*c* to produce 2.1% deformation.

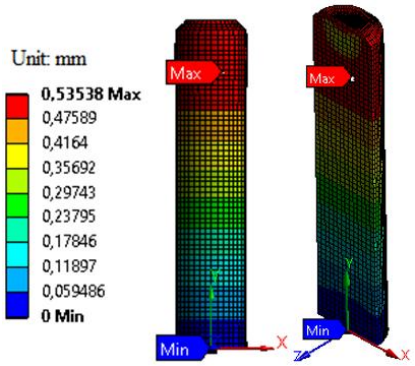

(a)

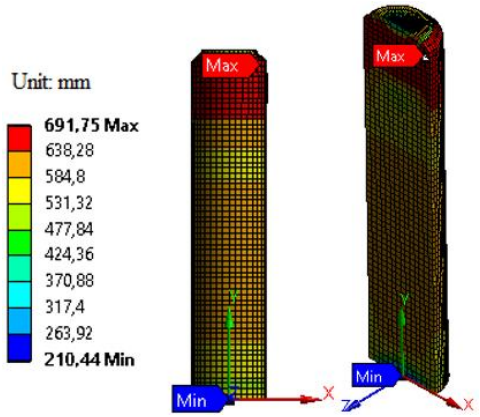

(b)

Figure 10. Deformation and stress solution results obtained using combined model, (a) Deformation results in the last step, (b) Hill 48 stress distribution in the last step

6. RESULTS AND DISCUSSIONS

Table 8, 9 and 10 show the values obtained as a result of optimization.

Table 8. Estimated parameters obtained from monotonic true stress true plastic strain data.

	Bilinear isotropic hardening		Chaboche's kinematic hardening					
Model	E (MPa)	YS(MPa)	C_1(MPa)	γ_1	C_2(MPa)	γ_2	C_3(MPa)	γ_3
Bilinear	801.56	495.73	--	--	--	--	--	--
Chaboche	--	364.99	32001.38	650.89	24001.78	501.89	23998.85	498.55
Combine	50.55	365.69	32000.38	650.05	24000.19	500.34	24000.85	500.71

Table 9. Estimated parameters obtained from the monotonic true stress true plastic strain data when no die is used.

	Bilinear isotropic hardening		Chaboche's kinematic hardening					
Model	E (MPa)	YS (MPa)	C_1 (MPa)	γ_1	C_2 (MPa)	γ_2	C_3 (MPa)	γ_3
Bilinear	6300.51	455.44	--	--	--	--	--	--
Chaboche	--	375.45	76000.28	800.79	1000.37	20.01	3000.61	20.93
Combine	5000.5	350.15	54000.81	1500.69	54000.19	1500.37	54000.69	1500.14

Table 10. Estimated parameters obtained from cyclic actual stress true plastic strain data.

	Bilinear isotropic hardening		Chaboche's kinematic hardening					
Model	E (MPa)	YS(MPa)	C_1(MPa)	γ_1	C_2(MPa)	γ_2	C_3(MPa)	γ_3
Bilinear	4100.79	320.33	--	--	--	--	--	--
Chaboche	--	120.12	280000.64	5000.41	36000.37	90.51	10000.72	90.83
Combine	10.54	100.90	280000.19	5000.66	36000.15	90.27	10000.48	90.59

In Figure 11, the experimental data and predicted curves are compared with each other using optimised material parameters. Neither the bilinear model nor the Chaboche models fit the experimental data well. Curves show that the combined model has the best improved fit of the models of experimental points.

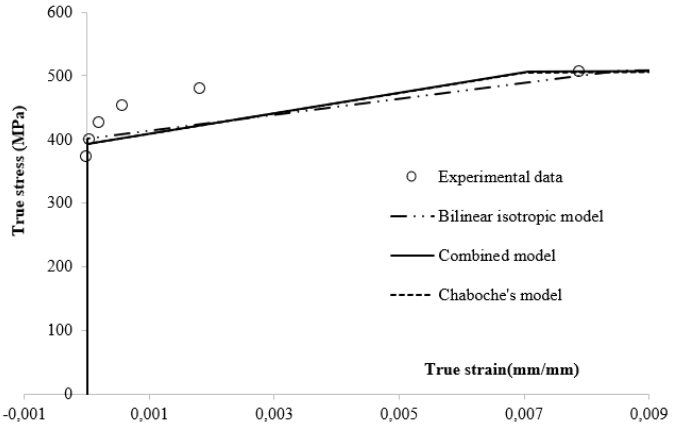

(a)

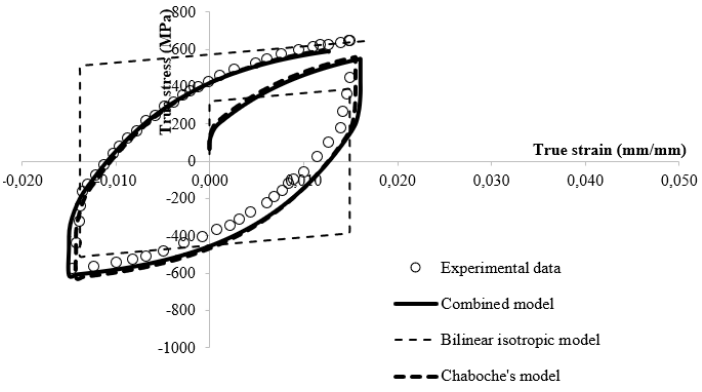

(b)

Figure 11. Estimated performances of the optimum models obtained for monotonic / cyclic loading conditions compared to experimental data (*a*) Monotonic model estimates (*b*) Cyclic model estimates

Figure 12 shows model predictions when monotonic models are used in cyclic deformation processes and vice versa. It is not seen to be well-fit to experimental data.

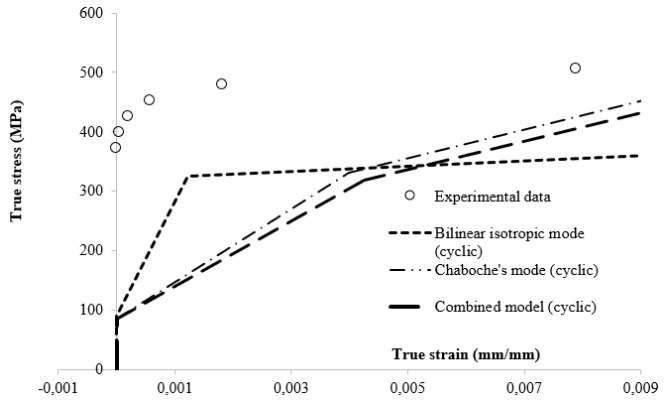

(a)

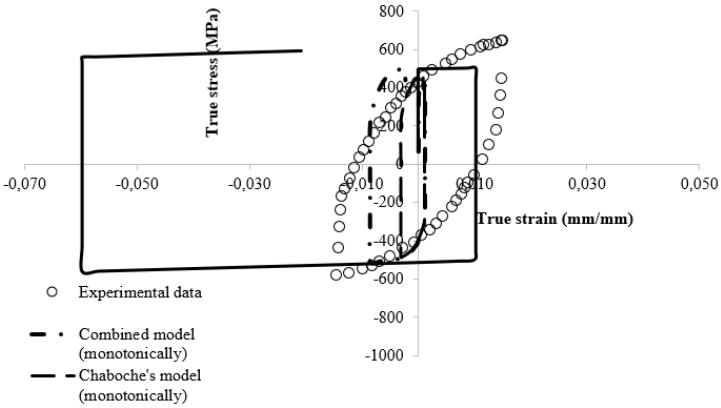

(b)

Figure 12. (a) Use of cyclic models in a monotonic deformation process. (b) Use of monotonic models in a cyclic deformation process

Figure 13 shows the curves in which the monotonic drawing process is not used using the values in Table 9.

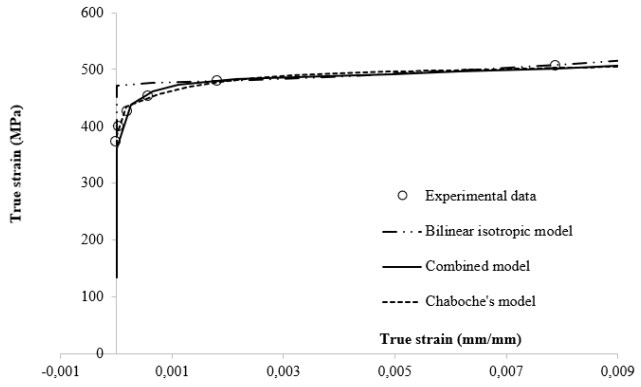

Figure 13. Estimated performance of the optimum models compared to the experimental data obtained when the die is not used for the monotonic loading case

Table 11. Models and parameters used in literature

	E^t (MPa)	YS (MPa)	C_1(MPa)	γ_1	C_2(MPa)	γ_2	C_3(MPa)	γ_3
In this study	50000	175	50000	5	17000	50	50000	175
Marini [24]	--	370	75000	460	--	--	--	--
LihuiLang [25]	433891.034	70	--	--	--	--	--	--
Agius [26]	--	112-441	68-187	4.885-468	--	1-889	102-7375	--

7. CONCLUSIONS

Some plasticity models are set using isotropic/kinematic hardening rules in the Hill48 yield criterion with an associated flow rule for FE simulation of a pipe drawing process. In this study, the optimization process is performed to determine and calibrate the plasticity model's parameters with monotonic and cycling stress-strain hardening curves. The results revealed that the drawed diameter can be predicted more accurately when the combined model parameters are used. Although there is a small difference between the experimental and the models' hysteresis loops, the diameter predictions are closer to the experimental results. The main findings obtained from investigations are listed below:

- The Hill48 criterion has predicted the stress values more accurately than von Mises. Due to anisotropy, the prediction ability of the Hill48 model is greater than von Misses.

- While a bilinear isotropic hardening rule by itself may be enough to predict the material behavior, which just includes a monotonic loading case, only a kinematic model or a bilinear isotropic model are not enough to simulate the cyclic plastic deformation process. Because it includes both isotropic and kinematic hardening together. So it is seen that the combined models provide more accurate predictions for monotonic and/or cyclic loadings.

- In the combined model, the elevated YS makes the loop expanded. While E^t is decreasing, the slope of the boundary curve also decreases. While C's are getting increased, the roundness of the vertices of the loop increases. While γ's are getting increased, the slope of the boundary curve decreases. The initial yield stress of the material YS has not had any effect on the error minimization performed by the curve-fitting tool.

- The coefficients optimized for the monotonic hardening curves are not suitable for prediction of cyclic loops.

REFERENCES

[1] Leonardo Kyo Kabayama, Simone Pereira Taguchi, Gustavo Aristides Santana Martinez, The Influence of Die Geometry on Stress Distribution by Experimental and FEM Simulation of Electrolytic Copper Wiredrawing, Materials Research, Vol.12, No.3, 281-285, (2009).M. Young, The Technical Writer's Handbook. Mill Valley, CA: University Science, 1989.

[2] Onur Duman, Mustafa Kemal Külekçi, Ultrasonik Titreşimin Tel Çekme İşlemine Etkisi, Pamukkale Üniversitesi Mühendislik Bilimleri Dergisi, 25 (4), 440-443, (2019).

[3] Andrea Panteghini, Francesco Genna, An engineering analytical approach to the design of cold wire drawing processes for strain-hardening materials, 3:279-289, (2010).

[4] Ioana Monica Sas-Boca, Marius Tintelecan, Mariana Pop, Dana-Adriana Iluţiu-Varvara, Adriana Maria Mihu, The Wire Drawing Process Simulation and the Optimization of Geometry Dies, 10th International Conference Interdisciplinarity in Engineering, 181, 187-192, (2017).

[5] Adriana-Maria Mihu, Ioana Monica Sas-Boca, Ionut Marian, Iulian Sebastian Mihu, Dorina Simona Ianc, Liviu Nistor, Dana-Adriana Ilutiu-Varvara, Finite Element Analysis of Drawing Wire in Cassette Roller Die, 9th International Conference Inderdisciplinarity in Engineering, 22, 34-39, (2016).

[6] L. Filice, G. Ambrogio, F. Guerriero, A multi-objective approach for wire-drawing process, 8th CIRP Conference on Intelligent Computation in Manufacturing Engineering, 12, 294-299, (2010).

[7] C. J. Luis, J. León, R. Luri, Comparison between finite element method and analytical methods for studying wire drawing processes, Journal of Materials Processing Technology, 164-165, 1218-1225, (2005).

[8] Ümit Şenyürek, Hüseyin Cömert, Tel Çekme Prosesi ve İnklüzyon Hasarları, SAU Fen Bilimleri Enstitüsü Dergisi, 6. Cilt, 3. Sayı, 178-182, (2002).

[9] Kazunari Yoshida ve Hiroaki Furuya Mandrel drawing and plug drawing of shape-memory-alloy fine tubes used in catheters and stents, Journal of Materials Processing Technology, 153–154 (2004) 145–150

[10] H. Pelletier ve ark. Limits of using bilinear stress]strain curve for finite element modeling of nanoindentation response on bulk materials, Thin Solid Films 379, 2000, 147-155

[11] Feng Lua ve Jinquan Xu Evaluation of cyclic inelastic response in fretting based on unified Chaboche model, International Journal of Fatigue 27 (2005) 1062–1075

[12] S. Sreenivasan, Serimant Kumar Mishra, Krishna Dutta, Ratceting strain and its effect on low cycle fatigue behavior of Al 7075-T6 alloy

[13] K. Saanouni, J.L. Chaboche, 3.06 –"Computational Damage Mechanics: Application to Metal Forming Simulation" Comprehensive Structural Integrity, Pergamon, 2003, Pages 321-376,

[14] Kacar, İ. and S. Kılıç, Pekleşme Kuralları, in Mühendislik Alanında Yenilikçi Yaklaşımlar, P.D.T. Güngör, et al., Editors. 2018, Gece Kitaplığı: ANKARA / TURKEY. p. 175-194.

[15] V.M.J. Sharma, G.S. Rao, S.C. Sharma, K.M. George, LowCycleFatigueBehaviour of AA2219-T87 at RoomTemperature, Materials Performance and Characterization 3(1) (2014) 103-126.

[16] İ. Kacar, S. Toros, Buckling Prevention Conditions on Cyclic Test Samples, in: M. Özcanlı, H. Serin, A. Çalık (Eds.) BucklingPrevention Conditions on Cyclic Test Samples, Çukurova Üniversitesi, Adana, 2016, pp. 4791-4798.

[17] D.R. Bland, The associated flow rule of plasticity, Journal of the Mechanics and Physics of Solids, Volume 6, Issue 1, 1957, Pages 71-78

[18] R. Hill, A theory of the yielding and plastic flow of anisotropic metals, Proceedings of the Royal Society of London. Series A. Mathematical and Physical Sciences 193(1033) (1948) 281-297.

[19] R. Hill, A theory of the yielding and plastic flow of anisotropic metals, Proceedings of the Royal Society of London. Series A. Mathematical and Physical Sciences 193(1033) (1948) 281-297.

[20] Support_Ansys, Video Demo: Material Curve Fitting, 2016. https://support.ansys.com/staticassets/ANSYS/staticassets/techmedia/material_curve_fitting.html.

[21] Sharcnet(c). 32.2. Modeling. 2018; Available from: https://www.sharcnet.ca/Software/Ansys/16.2.3/enus/help/ans_tec/teccurvefitchabmodel.html.

[22] Mohsen Safaeii Wim De Waele, Shun-lai Zang, Evoluationof Associated and Non-Associated Flow Metal Plasticity; Application for DC06 Deep Drawing Steel, Key Engineering Materials Vols. 504-506 (2012) pp 661-666.

[23] Irfan Kaymaz, Application of kriging method to structural reliability problems, Structural Safety 27 (2005) 133–151

[24] M. Marini, V. Fontanari, M. Bandini, M. Benedetti Surface layer modifications of micro-shot-peened Al-7075-T651, Experiments and stochastic numerical simulations, Surface & Coatings Technology 321 (2017) 265–278

[25] Lihui Lang ve ark. Pressure rate controlled unified constitutive equations based on microstructure evolution for warm hydroforming, Journal of Alloys and Compounds 574 (2013) 41–48

BIOGRAPHIES

Name Surname: Burak DEVECIOGLU
Address: Hayriye District, Tuzcular Street No: 22/6 Eskişehir/TURKEY

Name Surname: Erhan CELIK
Address: Asagi Hisar Street 4599. Sk. No: 15/3 Antalya/ Manavgat/TURKEY

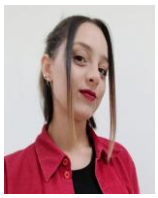

Name Surname: Merve ERTUGRUL
Address: Mimar Sinan District, Yunus Emre Street No: 26/1 Istanbul/TURKEY